

# Defects and lattice distortions in the superionic conductor



F. Kadlec<sup>a,b,\*</sup>, F. Moussa<sup>c</sup>, P. Simon<sup>a</sup>, G. Gruener<sup>a</sup>, B.P. Sobolev<sup>d</sup>

<sup>a</sup> CNRS–CRMHT, 45071, Orléans Cedex 2, France

<sup>b</sup> Institute of Physics, Czech Academy of Sciences, Na Slovance 2, 180 40, Praha 8, Czech Republic

<sup>c</sup> Laboratoire Léon Brillouin (CEA–CNRS), CEN Saclay, 91191 Gif sur Yvette Cedex, France

<sup>d</sup> Institute of Crystallography, Academy of Sciences of the Russian Federation, 117 333 Moscow, Russia

Received 28 September 1998

## Abstract

Diffuse neutron scattering (DNS) experiments have been performed on a single crystal sample of  $\text{Ba}_{0.84}\text{La}_{0.16}\text{F}_{2.16}$  at temperatures from 600 to 1000°C. The results confirm that the defects form clusters and cluster aggregates, the concentration of which diminishes upon heating. Furthermore, the data yield information about local lattice deformations and suggested that the mobile fluorine ions move in the closest vicinity of clusters, in agreement with the enhanced ionic motion model. Quenching is shown to influence the defect structure and the ionic conductivity. © 1999 Elsevier Science S.A. All rights reserved.

*Keywords:* Defects; Fluorides; Neutron scattering; Superionic conductivity

## 1. Introduction

It is known that in the fluorite structure crystals  $\text{MF}_2$  ( $M = \text{Ca}, \text{Sr}, \text{Ba}$ ), the doping by trivalent rare-earth elements R substantially enhances the disorder and ionic conductivity (see, e.g. [1,2]). The general chemical formula of these solid solutions reads  $(\text{MF}_2)_{1-x}(\text{RF}_3)_x$ . The overall cubic crystal symmetry (space group  $\text{Fm}\bar{3}\text{m}$ ) is conserved within  $0 \leq x < x_{\text{max}}$  where  $x_{\text{max}} \approx 0.4\text{--}0.5$  depending on M and R [3]. Like in the pure fluorite structure crystals, the conductivity is due to hopping of mobile  $\text{F}^-$  anions. The ions of rare-earth elements R substitute the M atoms and near every substitutional atom, there is one charge-compensating  $\text{F}^-$  anion at an interstitial site.

At heavy doping (approximately  $x > 0.01$ ), the crystal defects gather into clusters, the structure of which depends, in general, on M and R [4,5]. The lattice in the vicinity of the clusters is deformed, which leads to so-called defect regions [6] in the undeformed fluorite lattice. Based on calculations, such deformations in  $\text{CaF}_2$  have been estimated earlier to be of the order of

several percent of the lattice constant and to be limited to the atoms in the close vicinity of the defect [7]. According to the enhanced ionic motion model [8], these distortions are supposed to enhance the ionic conductivity by decreasing locally the value of the activation enthalpy for hops of  $\text{F}^-$  ions. This provides an easy conduction path for them in the closest vicinity of the clusters.

An important evidence about the cluster structure and configuration in the  $(\text{BaF}_2)_{1-x}(\text{LaF}_3)_x$  single crystals was obtained earlier by diffuse neutron scattering (DNS) experiments [9,10]. The authors have measured the scattered intensity on samples with  $x = 0.209$  and  $x = 0.492$ . In [10], room temperature DNS contour maps for these samples were published. These results were obtained in the scattering plane which contains  $\langle 100 \rangle$ ,  $\langle 110 \rangle$  and  $\langle 111 \rangle$  equivalent directions. Apart that, the temperature dependence of the intensity of a selected diffuse peak (with momentum transfer  $\vec{Q} = [2.69 \ 0 \ 0]$ ) was measured for temperatures up to 900°C. From the analysis of these dependences and from simulations of the DNS contour maps, the following main conclusions were drawn:

- The clusters in the  $\text{Ba}_{1-x}\text{La}_x\text{F}_{2+x}$  systems are of the 2:2:2 type (see Fig. 1).

\* Corresponding author. Tel.: +42-2-66052144; fax: +42-2-821227; e-mail: kadlec@fzu.cz.

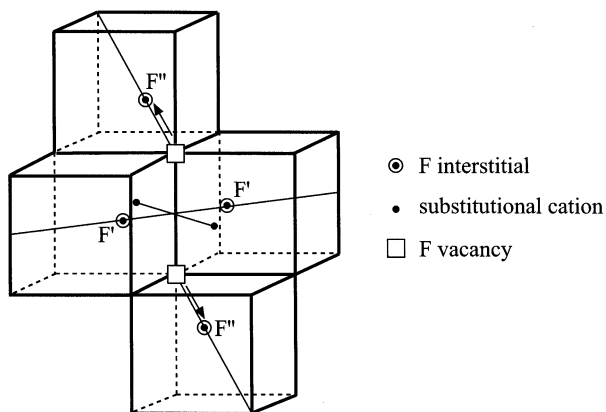


Fig. 1. The 2:2:2 cluster [10]; the unmarked corners of the cubes are occupied by fluorine ions of the regular lattice. The arrows mark the fluorine ion displacements accompanying the cluster formation (for details see text).

- The clusters form aggregates which comprise clusters aligned along the  $\langle 100 \rangle$  directions; an example is shown in Fig. 2. At room temperature, there are on average four clusters per aggregate. Within the aggregate, the distances between cluster centres are  $3a/2$  along the aggregate axis and  $a/2$  in one of four perpendicular  $\langle 100 \rangle$  directions. The directions of these transverse displacements are random.
- The mean number of clusters involved in the aggregates decreases on heating. This is evidenced by the decrease of the intensity at  $\vec{Q} = [2.69\ 0\ 0]$  with increasing temperature. The most significant drop is observed between 500 and 750°C. This interval coincides with an anomalous (i.e. faster than Arrhenius-like) increase in the conductivity. Based on this coincidence, the authors suggest a relation between the short range correlations between the clusters (aggregates) and the conductivity.

In the present article, we report results of DNS experiments obtained on a sample with a lower La concentration,  $x = 0.16$ . We were scanning in the vicinity of  $\vec{Q} = [2\ 2\ 1]$ , along the direction of aggregate

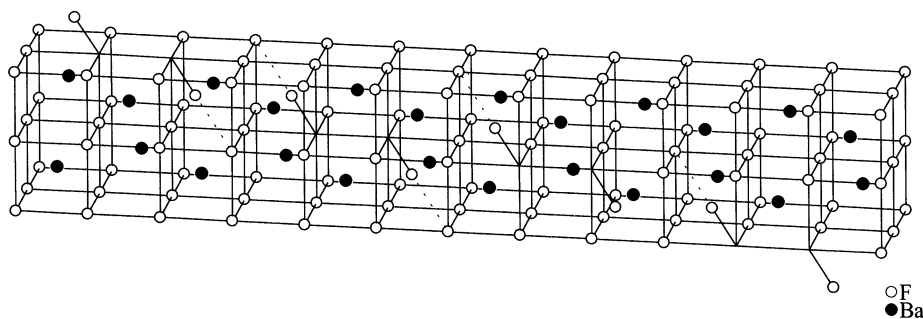


Fig. 2. Example of an aggregate of 2:2:2 clusters in  $(\text{BaF}_2)_{1-x}(\text{LaF}_3)_x$  at heavy doping, as shown by DNS [10]. For clarity, substitutional La ions are omitted and only the fluorine ions displaced from their lattice sites to interstitial  $F''$  positions are shown from the clusters. The dotted lines show the  $\langle 111 \rangle$  directions of these displacements. The picture does not take into account the lattice distortions around clusters (see also Fig. 7). Note that the size of the cubes is half of the lattice constant, so only six fcc unit cells are shown.

axes,  $[0\ 0\ 1]$ , as a function of temperature. These results make it possible to study local lattice deformations in this direction. Our results support the above statements and yield further information about the defect structure. Related results of inelastic scattering experiments, showing vibrational modes with  $\vec{q} = [0\ 0\ q_i]$ , localized around aggregates, are reported separately elsewhere [11].

## 2. Experimental

### 2.1. Neutron scattering

The single crystalline sample of  $\text{Ba}_{0.84}\text{La}_{0.16}\text{F}_{2.16}$  was grown from melts by the Bridgman technique [12] under fluorinating atmosphere in the Institute of Crystallography, Moscow. It had a cube-shaped form with a size of  $6 \times 6 \times 4\ \text{mm}^3$ . Its composition was verified by means of electron microprobe connected to an electron microscope. The doping rate was established with an accuracy better than  $\pm 0.5\%$ .

DNS experiments were performed at the reactor Orphée in the Laboratoire Léon Brillouin, Saclay on the triple-axis spectrometers 4F1 and 1T1. Pyrolytic graphite crystals were used as the monochromator and analyser. The sample was mounted in a high-vacuum aluminium furnace using a niobium sample holder and heated up to 1000°C. The scans were performed at a fixed incident wave vector of  $\lambda = 2.662\ \text{Å}$  and momentum transfer  $\vec{Q} = [2\ 2\ Q_1]$  within  $0 \leq Q_1 \leq 1.26$  (spectrometers' experimental limit).

First, the DNS spectra of the as-grown sample were recorded on heating at temperatures  $600 \leq T \leq 1000^\circ\text{C}$  on the spectrometer 4F1. After the experiment, the sample was cooled down to ambient temperature. The cooling rate of ca.  $10^\circ\text{C}\ \text{min}^{-1}$  was determined by the thermal capacity of the furnace. Subsequently, the DNS of the quenched sample was measured on the spectrometer 1T1.

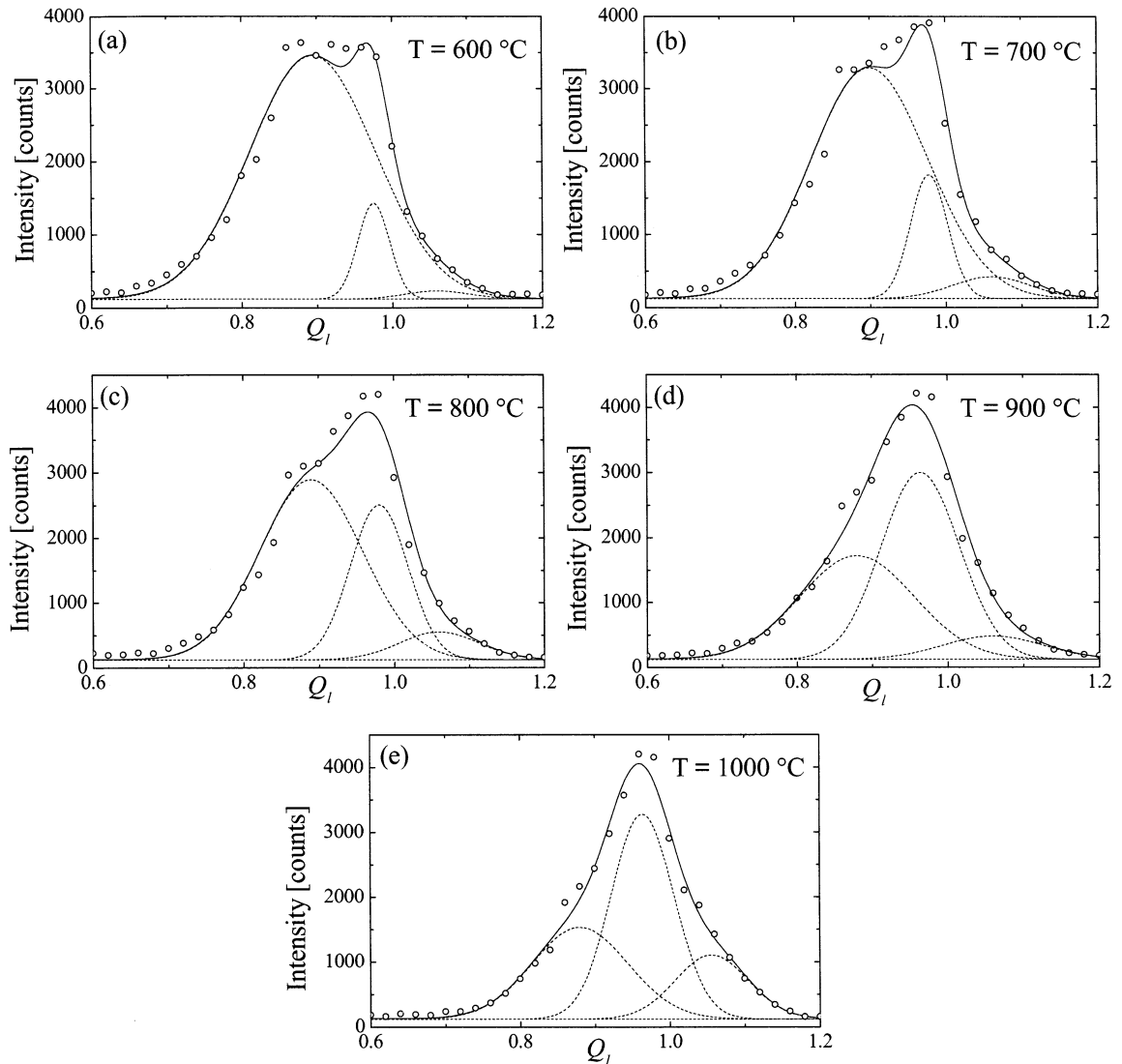


Fig. 3. DNS spectra of the as-grown sample, measured in the  $[2\ 2\ Q_1]$  direction at temperatures from 600 to 1000°C. Open circles: experimental points; solid line: calculated curve; dashed lines—contributions of individual terms.

## 2.2. Conductivity measurements

Room temperature conductivity of the quenched sample was measured using a HP 4194 A complex impedance analyzer in the frequency range  $100\text{ Hz} \leq \omega \leq 1\text{ MHz}$ . Silver paste electrodes were deposited on two opposite faces of the sample and silver wires were used for connections.

## 3. Results and evaluation

### 3.1. Neutron scattering

The measured  $\vec{Q} = [2\ 2\ Q_1]$  scans of the as-grown sample are shown by symbols in Fig. 3. The Bragg peak  $\vec{Q} = [2\ 2\ 0]$  and the region of flat background level  $0 \leq Q_1 \leq 0.6$  are omitted.

Near  $Q_1 = 1$  an intense DNS signal was observed. This is a striking effect, as in the face centred cubic (fcc) structure, the  $[2\ 2\ 1]$  Bragg peak is forbidden, so no signal would be expected. If we compare the data obtained at different temperatures (see Fig. 4), we see that the intensity decreases with  $T$  for  $0.65 \leq Q_1 \leq 0.92$  while it increases with  $T$  in the region  $0.94 \leq Q_1 \leq 1.16$ . Furthermore, the latter interval can be divided in two: whereas below  $Q_1 = 1$ , the increase stops at  $T = 800^\circ\text{C}$ , above this value of  $Q_1$  the intensity grows up to  $T = 1000^\circ\text{C}$ .

In order to describe these features, we fitted the data near  $Q_1 = 1$  by three Gaussian curves, shown by dashed lines in Fig. 3. The same level of background noise (120 counts) was used for all the spectra. The fit results are shown by solid lines in Fig. 3. The aim of the fitting procedure was to find a set of parameters so that neither the centres of gravity of the peaks nor their

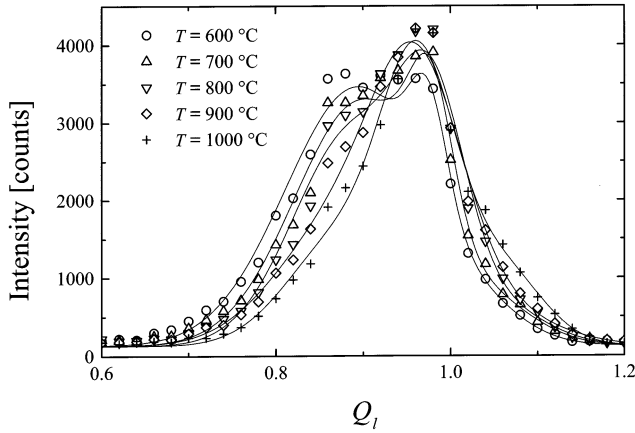


Fig. 4. Comparison of the experimentally obtained DNS spectra from Fig. 3 in the  $0.6 \leq Q_1 \leq 1.2$  region. Solid lines: curves calculated from fits.

widths change substantially with temperature. Therefore it appeared necessary to exclude some parameters from the automatic fitting procedure, however we tried to fix as few of them as possible. The temperature dependences of the resulting parameters are shown in Fig. 5.

The product  $GI$  of the peaks' intensity  $I$  and of their full width at half maximum  $G$  is proportional to the area below the peaks. Therefore, it describes the scat-

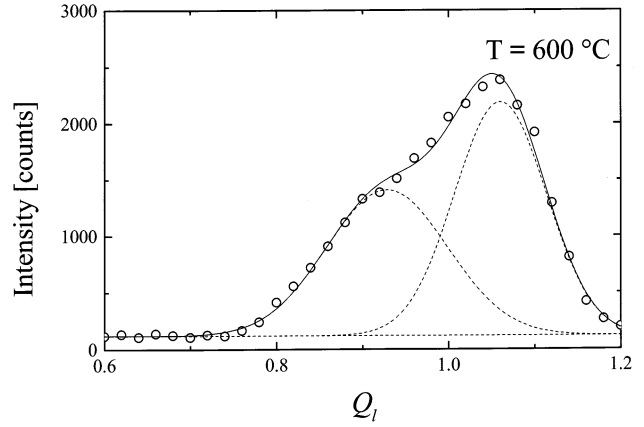


Fig. 6. DNS scan at  $Q_1 = [2 \ 2 \ Q_1]$  and  $T = 600^\circ\text{C}$  after sample quenching. (Note: the intensity is not comparable with that in Fig. 3 due to different sample volume).

tering volume responsible for individual parts of the signal.  $GI$  as a function of temperature is shown in Fig. 5b. We see that at  $T = 600^\circ\text{C}$ , almost all the signal comes from the peak centred at  $Q_1 \approx 0.9$ . Upon increasing temperature, the area below this peak diminishes whereas these below the other two peaks increase. We will discuss this behaviour in the following section.

The DNS spectrum obtained after quenching at  $T = 600^\circ\text{C}$  is shown in Fig. 6. The spectrum distinguishes itself from those of the as-grown sample especially by

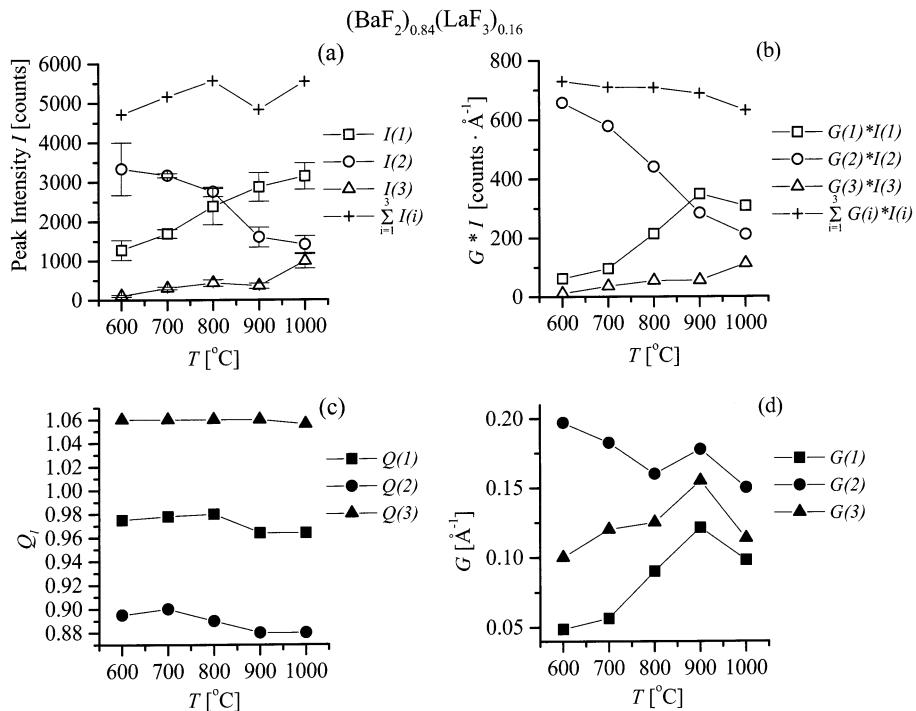


Fig. 5. Temperature dependences of the parameters used to fit the DNS spectra in Fig. 3: (a) peak intensities  $I$ ; (b) product of intensity  $I$  and peak width  $G$ ; (c) the coordinate  $Q_1$  of the peak centres; (d) full width at half maximum  $G$ . The parameters describe the peaks due to neutrons scattered from cluster aggregates ( $\circ$ ), interface zone ( $\triangle$ ) and individual clusters ( $\square$ ). The crosses in (a) and (b) show the total scattered intensity (sum of the three peaks). One can see that it does not change substantially with temperature which means that the scattered intensity originates at all temperatures approximately from the same volume fraction of the sample.

the relative intensity above  $Q_1 \approx 1$ . Although it appears possible to fit the data by three curves with the same positions as in the case of the as-grown sample, this approach is not justified by the shape of the experimental curve. Only two Gaussian peaks can be discerned clearly, one of them being located at  $Q_1 = 1.06$ , with an intensity obviously much higher than before annealing.

### 3.2. Conductivity measurements

The experimentally obtained room temperature impedance values  $Z(\omega) = Z'(\omega) + iZ''(\omega)$  of the quenched sample, plotted in the  $Z'(\omega) - Z''(\omega)$  complex impedance plane have yielded an expected shape close to a semi-circle. By extrapolation of the data to the real axis, the value of the static conductivity was determined as  $\sigma = (1.3 \pm 0.1) \times 10^{-8} (\Omega \text{ cm})^{-1}$ .

## 4. Discussion

Given the proximity of all observed peaks to  $Q_1 = 1$  (see Fig. 3), we assign this signal to the  $[2\ 2\ 1]$  Bragg peak, which is extinct in the fcc lattice of  $\text{BaF}_2$ . In this structure, the Bragg reflections  $[hkl]$  are limited to those where all the sums  $h+k$ ,  $k+l$  and  $h+l$  are even. However, in non-stoichiometric crystals, doping can activate some of reflections which do not fulfil these conditions, as the interstitial ions occupy crystal sites which are void in the fcc  $\text{BaF}_2$  lattice. As we see from Fig. 3, the shape of the  $[2\ 2\ 1]$  reflection is very different from a simple Bragg peak: first, its width (about  $0.2 \text{ \AA}^{-1}$ ) is larger than that of Bragg peaks convoluted with the spectrometer resolution (e.g. measured full width at half maximum of the  $[2\ 2\ 0]$  peak is about  $0.03 \text{ \AA}^{-1}$ ); second, there are the previously described three components. These features will be discussed below.

Our choice to fit the spectra of the as-grown sample by three Gaussian curves is not the only possible one: the peak centred at  $\approx 1.06$  is rather weak compared to the other two. Thus, it would be in principle possible to use only two peaks in the fit. Nevertheless, the presence of the third peak is strongly supported by the experimental data obtained on the quenched sample (Fig. 6).

As we mentioned above, all the trivalent rare earth ions are supposedly comprised in the 2:2:2 clusters. Therefore, we assume that the signal which reminds of the  $[2\ 2\ 1]$  peak comes just from the clusters or their closest vicinity where the lattice deviates from the fcc structure. At  $T = 600^\circ\text{C}$ , the majority of this signal is due to the Gaussian peak centred at  $Q_1 \approx 0.9$  (see Fig. 3a). In analogy with the model of the defect structure which was proposed in [9,10], we suppose that the clusters form aggregates at this temperature and below. As the centre of this peak lies below  $Q_1 = 1$ , in aggre-

gates, the local lattice constant is greater than that of the surrounding pure  $\text{BaF}_2$  matrix. The expansion factor in the real space is equal to  $1/Q_1 \approx 1.11$ . Thus, we have shown that the lattice within the aggregated clusters is expanded with respect to the pure fluorite matrix; the local lattice constant within the aggregates exceeds  $a$ , that of the matrix, by 11% on average.

In all the DNS spectra, there is another peak centred below  $Q_1 = 1$ , namely at  $Q_1 \approx 0.97$  (see Fig. 3a). In analogy with the above reasoning, we believe that it comes from the non-fcc parts of the sample where the lattice is expanded approximately by 3% on average. We suppose that here we have observed those of the 2:2:2 clusters which do not form aggregates. It seems obvious that the lattice expansion caused by individual clusters is smaller than that induced by aggregates of them. We assume that the width of this peak ( $G \approx 0.05 \text{ \AA}^{-1}$  at  $600^\circ\text{C}$ ) reflects a characteristic length of the short range order between individual clusters, i.e., the system can be regarded as a perturbed averaged lattice.

The local lattice expansion due to doping is shown in a schematic way in Fig. 7. From this simplified picture we can see that between the cluster or cluster aggregate (A) and the pure fcc  $\text{BaF}_2$  matrix (C), there is an interface zone (B). This zone occupies a certain volume of the sample and we see from Fig. 7 that here the unit cells have, in turn, a reduced volume with respect to the matrix (C). We suppose that the interface zone is at the origin of the DNS signal which we fitted by the third peak, centred at  $Q_1 \approx 1.06$ . The inverse of this value is about 0.94, which means that the local lattice constant in the interface region is reduced, on average, by about 6% with respect to  $a$ .

Of course, it is necessary to answer the question which ions represent the defects of the fcc structure within the interface so that we see the  $[2\ 2\ 1]$  Bragg reflection from this region (at  $Q_1 \approx 1.06$ ). As we suppose that all dopant ions are bound inside the clusters, a possible explanation is that this DNS signal is due to

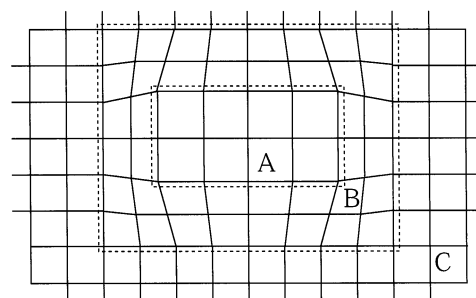


Fig. 7. Sketch of the lattice distortions caused by clusters: (A) cluster or aggregate of clusters—the lattice is expanded due to the presence of dopant ions; (B) interface zone—the deformed fluorite structure lattice (without dopant ions); note that the lattice is essentially compressed with respect to the matrix (C); (C) undeformed lattice.

the  $F^-$  anions which move in the closest vicinity of the clusters, in void sites of the  $BaF_2$  structure. This is an assumption which was made in the enhanced ionic motion model [8]. The reason can also possibly consist in the fact that in the B region, the lattice is not rigorously cubic (see Fig. 7), so the extinction rules for the Bragg peak are broken in this region.

Next, we will analyze in some detail the temperature behaviour of the parameters given by the fits. If the above interpretation is correct then as we see from Fig. 3, at  $T = 600^\circ\text{C}$ , most clusters are bound to aggregates; on heating, the peak due to aggregates diminishes. By contrast, the perturbed average lattice signal induced by individual clusters around  $Q_1 \approx 0.98$  increases. It means clearly that the aggregates disintegrate into individual clusters. As we can see from Fig. 5b, there is a crossover of the integral intensities just below  $900^\circ\text{C}$  and above this temperature, the volume fraction of the individual clusters exceeds that of cluster aggregates. In agreement with the assumption that the aggregates disintegrate in individual clusters, the peak due to the interface (around  $Q_1 \approx 1.06$ ) also increases with temperature.

We see in Fig. 5b that between  $900$  and  $1000^\circ\text{C}$ , the integral intensity of the peak due to individual clusters decreases. This might be caused by the fact that the clusters exert vibrations the frequency of which increases with temperature. If the frequency approaches the limit of the experimental frequency window (ca.  $0.25 \leq \omega \leq 0.25$  THz), the detected signal loses its quasistatic character and diminishes. In [9,10], the authors suppose that the correlation between the clusters diminishes especially in the temperature region from  $600$  to  $800^\circ\text{C}$ . Our results lead to a similar conclusion: below  $T = 600^\circ\text{C}$ , the majority of the clusters are in aggregates and the volume fraction of individual clusters is relatively small. The loss of cluster correlation occurs progressively in the whole temperature region measured, i.e. from  $600$  to  $1000^\circ\text{C}$ .

The modification of the DNS spectrum after quenching (see Fig. 6) shows that the defect structure was changed by the thermal treatment. Compared to the as-grown sample (Fig. 3), one can see that the relative intensity of the peak due to compressed lattice has grown by about one order of magnitude due to quenching. This shows that the short-range configuration of defects is different from that in the as-grown sample. We assume that there is a significant increase in the concentration of independent clusters and the volume of interface of defects (zone B in Fig. 7), which is assumed to be a zone of enhanced conductivity. In accordance, the value of the room temperature conductivity after quenching  $\sigma = 1.6 \times 10^{-8} (\Omega \text{ cm})^{-1}$  is about five times higher than that of as-grown samples ( $\sigma \approx 3.3 \times 10^{-9} (\Omega \text{ cm})^{-1}$  [13]). Another aspect of these supposed changes with quenching would be that the

mean number of clusters per aggregate is lower than in the as-grown sample. Accordingly, results of recent experiments (not yet published) reveal a decrease of intensity of localized vibrations in the inelastic spectra after quenching.

## 5. Conclusions

We have shown that, in agreement with the enhanced ionic motion model [8], doping causes local lattice deformation within the  $Ba_{0.84}La_{0.16}F_{2.16}$  crystals: the local lattice constant within individual clusters and cluster aggregates exceeds the long-range lattice constant  $a$  by 3 and 11%, respectively. This expansion is compensated by a local compression within the interface zone by about 6% with respect to  $a$ . With increasing temperature, the cluster aggregates disintegrate into individual clusters. The presence of the DNS peak at  $[2\ 2\ 1.06]$  may be related to the fact that the hopping fluorine ions move in the interface zone. Quenching manifests itself by a significant increase of this peak and by a conductivity enhancement. These are apparently consequences of changes in the defect structure, namely decreased spatial coherence between clusters within aggregates.

## Acknowledgements

We would like to express our thanks to K. Jurek from the Institute of Physics for establishing the exact composition of the sample. One of the authors (F.K.) acknowledges a scholarship of the French Ministry of Foreign Affairs. The work was supported by Czech grant agencies (GA AV project No. A1010517 and GAČR project No. 202/95/1393).

## References

- [1] D. Grandjean, T. Challier, D.J. Jones, P. Vitse, *Solid State Ionics* 51 (1992) 297–303.
- [2] A.K. Ivanov-Shits, N.I. Sorokin, P.P. Fedorov, B.P. Sobolev, *Solid State Ionics* 31 (1989) 269–280.
- [3] B.P. Sobolev, *Buttl. Soc. Cat. Cièn. XII* 2 (1991) 275–332.
- [4] J.M. Réau, P. Hagenmuller, *Appl. Phys. A* 49 (1989) 3–12.
- [5] S.V. Chernov, W. Gunßer, I.V. Murin, *Solid State Ionics* 47 (1991) 67–70.
- [6] A.K. Ivanov-Shits, N.I. Sorokin, P.P. Fedorov, B.P. Sobolev, *Solid State Ionics* 31 (1989) 253–268.
- [7] T.M. Haridasan, J. Govindarajan, M.A. Nerenberg, P.W.M. Jacobs, *Phys. Rev. B* 20 (8) (1979) 3462–3473.
- [8] K.E.D. Wapenaar, J. Schoonman, *J. Electrochem. Soc.* 126 (4) (1979) 667–672.
- [9] N.H. Andersen, K. Clausen, J.K. Kjems, Defect structure, thermal properties and ionic conductivity of heavily doped fluorites, in: F.W. Poulsen et al. (Eds.), *Transport–Structure Relations in Fast Ion and Mixed Conductors*, The 6th Risø International

- Symposium on Metallurgy and Materials Science, 1985, pp. 171–182.
- [10] N.H. Andersen, K.N. Clausen, J.K. Kjems, J. Schoonman, J. Phys. C Solid State Phys. 19 (1986) 2377–2389.
- [11] F. Kadlec, F. Moussa, P. Simon, B.P. Sobolev, Solid State Ionics (submitted for publication).
- [12] A.K. Ivanov-Shits, N.I. Sorokin, P.P. Fedorov, B.P. Sobolev, Fiz. Tv. Tela 25 (6) (1983) 1748–1753.
- [13] R.A. Panhuyzen, A.F.M. Arts, K.E.D. Wapenaar, J. Schoonman, Solid State Ionics 5 (1981) 641–644.